Demonstrating Path-Independent Anyonic Braiding on a Modular Superconducting Quantum Processor

Jingjing Niu,[1,2,3,4,*,†] Yishan Li,[5,*] Libo Zhang,[1,2,3,*] Jiajian Zhang,[1,2,3] Ji Chu,[1,2,3] Jiaxiang Huang,[1,2,3] Wenhui Huang,[1,2,3] Lifu Nie,[1,2,3] Jiawei Qiu,[1,2,3] Xuandong Sun,[1,2,3] Ziyu Tao,[1,2,3] Weiwei Wei,[1,2,3] Jiawei Zhang,[1,2,3] Yuxuan Zhou,[1,2,3] Yuanzhen Chen,[1,2,3,5] Ling Hu,[1,2,3] Yang Liu,[1,2,3] Song Liu,[1,2,3,4] Youpeng Zhong,[1,2,3,4,‡] Dawei Lu,[1,2,3,5,§] and Dapeng Yu[1,2,3,4,5]

[1]*Shenzhen Institute for Quantum Science and Engineering, Southern University of Science and Technology, Shenzhen 518055, China*

[2]*International Quantum Academy, Shenzhen 518048, China*

[3]*Guangdong Provincial Key Laboratory of Quantum Science and Engineering, Southern University of Science and Technology, Shenzhen 518055, China*

[4]*Shenzhen Branch, Hefei National Laboratory, Shenzhen 518048, China*

[5]*Department of Physics, Southern University of Science and Technology, Shenzhen 518055, China*

(Received 30 May 2023; revised 22 November 2023; accepted 1 December 2023; published 8 January 2024)

Anyons, exotic quasiparticles in two-dimensional space exhibiting nontrivial exchange statistics, play a crucial role in universal topological quantum computing. One notable proposal to manifest the fractional statistics of anyons is the toric code model; however, scaling up its size through quantum simulation poses a serious challenge because of its highly entangled ground state. In this Letter, we demonstrate that a modular superconducting quantum processor enables hardware-pragmatic implementation of the toric code model. Through in-parallel control across separate modules, we generate a 10-qubit toric code ground state in four steps and realize six distinct braiding paths to benchmark the performance of anyonic statistics. The path independence of the anyonic braiding statistics is verified by correlation measurements in an efficient and scalable fashion. Our modular approach, serving as a hardware embodiment of the toric code model, offers a promising avenue toward scalable simulation of topological phases, paving the way for quantum simulation in a distributed fashion.

DOI: 10.1103/PhysRevLett.132.020601

In recent years, a number of exotic quantum phases have been discovered that cannot be classified through traditional methods based on local order parameters and spontaneous symmetry breaking [1–12]. Many of these topologically ordered phases are defined by the emergence of quasiparticles with long-range quantum entanglement, known as anyons [4,13,14]. Unlike bosons or fermions in three dimensions, exchanging their positions results in a generic phase factor instead of 1 or -1 for Abelian type anyons [15–17], or even a unitary operation that shifts the system between different topologically degenerate states for non-Abelian anyons [9–11,18–27]. A paradigmatic topological two-dimensional (2D) lattice model is the toric code model that exhibits $\mathbb{Z}_2$ topological order and anyonic excitations [8,28–37]. Given its inherent richness and potential applications in topological quantum computing, there has been extensive interest in experimentally realizing the toric code model [17,38–55]. Researchers have not only engineered topological ordered states and explored their nonlocal properties using quantum circuits [51] but also observed non-Abelian anyon exchange statistics [53,54].

Demonstrating the path-independent nature of the anyonic statistics not only provides a better understanding of braiding operations under realistic noise but also opens up the possibility of fully utilizing the advantages of anyonic statistics [56–60]. The path-independent nature has been realized in nuclear magnetic resonance [47], superconducting quantum circuits [39], and photons [43]. In these experiments, starting from the toric code ground state, anyonic excitations are created and nontrivial phases can be acquired depending on the braiding path on which the anyons are interchanged [61]. However, this leads to notable challenge when scaling up because the highly entangled ground state requires a large number of entangling gates to prepare.

Here, we show that a modular superconducting quantum processor provides hardware convenience for implementing the toric code model. Superconducting quantum processors have recently emerged as a promising platform for realizing scalable quantum computers [62–64], but they face engineering challenges such as insufficient wafer area and congested control line layout when scaling up [65,66]. The modular approach, where smaller modules are constructed separately and then assembled into a larger architecture, can effectively overcome these bottlenecks [67–72]. Taking advantage of the parallelism inherent in

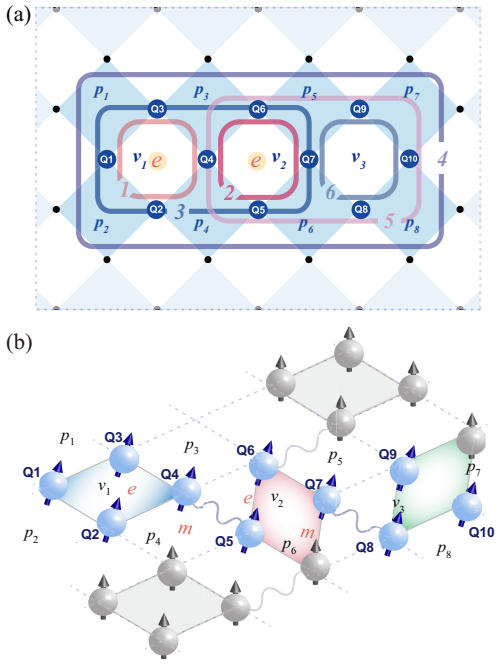

FIG. 1. (a) Square-lattice toric code model used, requiring a minimum of 10 qubits. It features three vertices and six paths: three nontrivial (in red) and three trivial (in blue). (b) Hardware embodiment of the toric code model on a modular superconducting processor.

the distributed architecture, we prepare a 10-qubit toric code ground state across three modules in four steps. Moreover, we develop a method using correlation measurements to extract phase information from each braiding path, enabling efficient and scalable verification of the path-independent anyonic statistics. Unlike previous demonstrations of parity oscillations [39,73,74], our new method employs a universal correlation curve for extracting necessary observables through the decomposition of Pauli components. This approach affords us the capability not only to define arbitrary measurement operators in accordance with system requirements, but also to calibrate complex entangled states extending beyond Greenberger-Horne-Zeilinger states.

We consider the square-lattice toric code model in Fig. 1(a). This specific configuration necessitates the utilization of at least ten qubits, which possess three unique vertices and six distinct paths, comprising three trivial and three nontrivial paths. Our modular processor serves as a hardware embodiment of this model, as shown in Fig. 1(b). Ten qubits labeled as Q_1 to Q_{10} across three modules are used in this experiment. The toric code Hamiltonian involves two kinds of four-body interactions, namely,

$$H = -\sum_v A_v - \sum_p B_p, \tag{1}$$

where $A_v = \prod_{i \in \mathrm{star}(v)} \sigma_x^i$ denotes the interaction among the four qubits on the star around each vertex v, and $B_p = \prod_{j \in \mathrm{edge}(p)} \sigma_z^j$ is on the boundary of each plaquette p. Because all the stabilizer operators commute with each other, the ground states $|\psi_g\rangle$ can be defined as the $+1$ common eigenstates of the A_v and B_p operators. A quasiparticle called e (m) particle is generated on vertex v (plaquette p) if A_v (B_p) acting on the resulting state $|\psi_e\rangle$ ($|\psi_m\rangle$) yields an eigenvalue -1. Four-body interactions are notoriously difficult to engineer experimentally in a controllable way. Since the anyon properties are associated with the underlying many-body entangled states only, instead of engineering the four-body interactions, one could alternatively generate the ground and excited states of the toric code model using quantum gates [61,75].

The ground state of this specific 10-qubit toric code is

$$\begin{aligned}|\psi_g\rangle = (&|0\rangle^{\otimes 10} + |0\rangle^{\otimes 6}|1\rangle^{\otimes 4} + |1\rangle^{\otimes 4}|0\rangle^{\otimes 6} \\ &+ |0001111000\rangle + |0001110111\rangle + |1111001111\rangle \\ &+ |1110111000\rangle + |1110110111\rangle)/2\sqrt{2}.\end{aligned} \tag{2}$$

Starting from the ground state in Eq. (2), a pair of e (m) particles are generated on the neighboring two vertices (plaquettes) by applying a σ_z (σ_x) rotation to a qubit. Anyonic statistics can be demonstrated between e and m particles by moving one around the other and acquiring a phase π along a closed-loop path. See the Supplemental Material [76] for more details.

We follow the circuit in Fig. 2(a) to generate the state $|\psi_g\rangle$ in Eq. (2). Taking advantage of the parallelism inherent in the modular architecture, the creation of this ground state is greatly simplified. As depicted in Fig. 2(a), two intermodule gates are applied simultaneously to create the Bell states $|\mathrm{Bell}\rangle_{45}$ and $|\mathrm{Bell}\rangle_{78}$ across the three modules. The instantaneous quantum state is characterized with quantum state tomography [77], yielding a state fidelity of 91.7%; see Fig. 2(b). Afterward, an intramodule entangled state $|\mathrm{Bell}\rangle_{12}$ is created, yielding $|\mathrm{Bell}\rangle_{12} \otimes |\mathrm{Bell}\rangle_{45} \otimes |\mathrm{Bell}\rangle_{78}$ with a state fidelity 85.2%; see Fig. 2(c). To efficiently verify quantum state preparation, we introduce the correlation measurement method. Simultaneously measuring correlation oscillation patterns for all qubits in the transverse plane, we extract the collective correlation operators $\mathcal{C}(\gamma) = \prod_{i=1}^{N} (\cos\gamma\sigma_y^i - \sin\gamma\sigma_x^i)$ with a tunable phase γ, as illustrated in Fig. 2(d). The ground state preparation process, depicted in Fig. 2(a), including entangled state calibration results from 4q to 10q, can be found in [76]. This correlation measurement method enables us to verify the ground state generation in an efficient and scalable fashion.

Now we explore the anyonic statistics after exciting two e particles in vertices v_1 and v_2. Under this setting, there are three π-phase-inducing loops with respect to these two e particles (Paths 1, 2, and 5), two loops that contain a pair of e particles (Path 3 and 4), and a trivial loop around v_3 without any e particle (Path 6). To perform the braiding

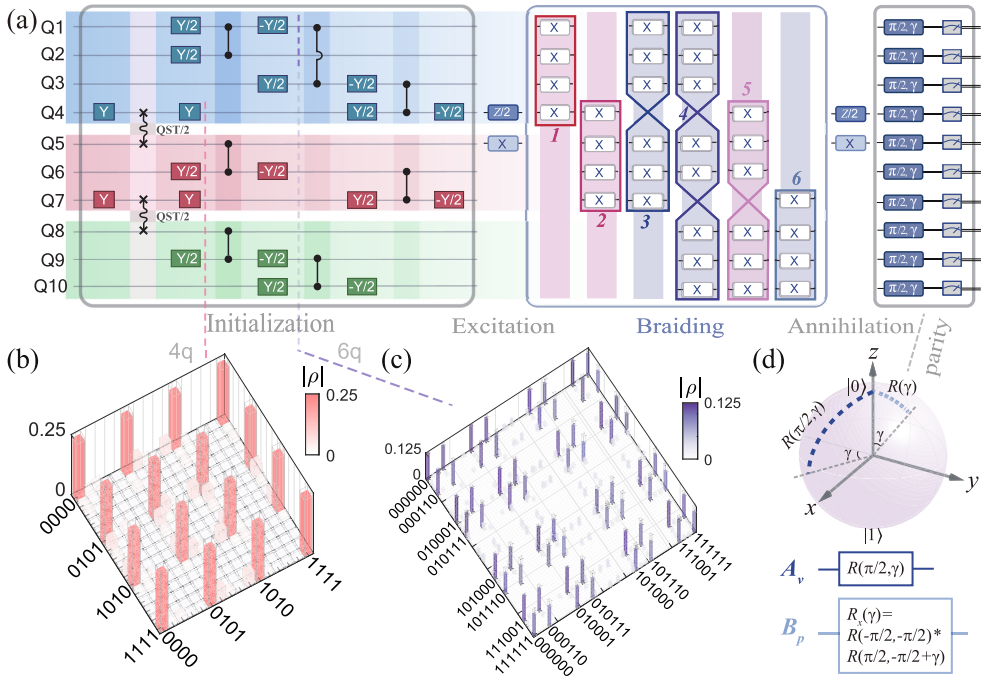

FIG. 2. (a) Quantum circuit for toric code ground state preparation, anyonic excitation, braiding, and annihilation. $\pm$Y/2 and Z/2 denote $R_y(\pm\pi/2)$ and $R_z(\pi/2)$ gates, respectively. Note only one braiding path is performed in each experiment. (b) The four-qubit intermodule entangled state $|\mathrm{Bell}\rangle_{45} \otimes |\mathrm{Bell}\rangle_{78}$ obtained through state tomography, with a state fidelity of 91.7%. (c) The six-qubit entangled state $|\mathrm{Bell}\rangle_{12} \otimes |\mathrm{Bell}\rangle_{45} \otimes |\mathrm{Bell}\rangle_{78}$, with a fidelity of 85.2%, where only $\mathrm{CNOT}^{\mathrm{Q1\text{-}Q2}}$ are operated in the second layer. (d) Correlation measurement scheme for the $\mathcal{C}_v$ and $\mathcal{C}_p$ operators.

operations, we excite a pair of m particles on the edge of the system so that they are involved in each loop. The nontrivial braiding phase $e^{i\pi}$ is a global phase of the system and is not directly measurable. A widely adopted scheme to manifest this phase is to use Ramsey-like interference [61], where a $Z/2$ gate is applied to Q_4 to generate an equal superposition of the ground state $|\psi_g\rangle$ and the excited state $|\psi_e\rangle$ before braiding, instead of simply applying a Z gate to excite a pair of e particles. A pair of m particles are excited in plaquettes p_4 and p_6 by applying an X gate to Q_5 as well; see the circuit in Fig. 2(a). The six braiding paths require different combinations of X gates, and only one path is implemented in each experiment. The last step is to annihilate the remaining particles the way they were created. For the trivial braiding paths (Paths 3, 4, and 6), the annihilation of the e particles results in a solid creation of the excited state $|\psi_e\rangle$ [61]. For the nontrivial braiding paths (Paths 1, 2, and 5), the loops generate a phase of $e^{i\pi}$ and the particles are perfectly annihilated. Assuming a more general phase factor $e^{i\theta}$, the resulting state is given by $|\psi\rangle = \frac{1}{2}[(1-e^{i\theta})|\psi_g\rangle - i(1+e^{i\theta})|\psi_e\rangle]$.

In the ideal case where the quantum state is pure, a complete set of the $\langle A_v\rangle$ and $\langle B_p\rangle$ values are sufficient to fully determine the state. However, the experimentally generated states are impure, and the quantum state readout is not perfect. Instead of simply measuring the stabilizers, we expand the stabilizers A_v and B_p into a set of correlation functions:

$$\mathcal{C}_v(\gamma) = \prod_{i\in \mathrm{star}(v)} \left(\cos\gamma\sigma_y^i - \sin\gamma\sigma_x^i\right),$$
$$\mathcal{C}_p(\gamma) = \prod_{j\in \mathrm{edge}(p)} \left(\cos\gamma\sigma_z^j + \sin\gamma\sigma_y^j\right). \quad (3)$$

Here, γ is a tunable rotating angle on each qubit. As shown in Fig. 2(d), single qubit rotation pulses $R(\pi/2,\gamma)$ and $R_x(\gamma) = R(-\pi/2,-\pi/2)R(\pi/2,\gamma-\pi/2)$ are applied to each qubit to measure the correlation operators $\mathcal{C}_v(\gamma)$ and $\mathcal{C}_p(\gamma)$ [76]. The selection of correlation operators aligns directly with the system's requirements, as our method necessitates no additional compromises. For instance, in arbitrarily larger ground states, adjusting the stabilizers as outlined in Eq. (3) will consistently fulfill the demands of subsequent data processing.

The correlation measurement results are shown in Fig. 3. The upper panel in Fig. 3(a) shows the results for measuring $\mathcal{C}_v(\gamma)$ at the vertex v_1. The results of the nontrivial paths (Paths 1, 2, and 5, in three different shades of red) are similar to that of the ground state (gray), while the results of the trivial paths (Paths 3, 4, and 6, in three different shades of blue) have opposite behaviors due to the lack of braiding phase $e^{i\pi}$.

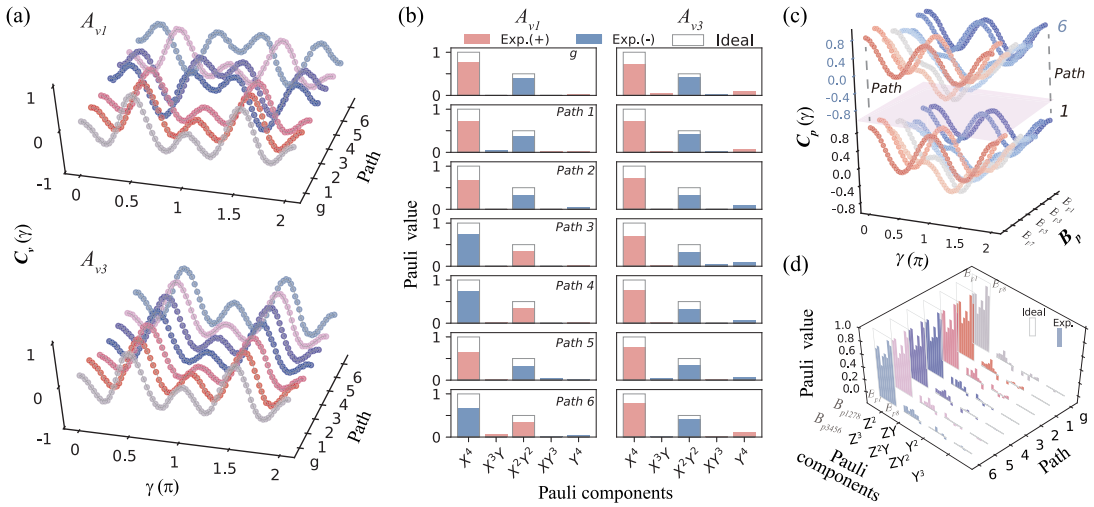

FIG. 3. (a) Correlation measurements at vertices v_1 (upper panel) and v_3 (lower panel) for six braiding paths. (b) Extracted Pauli components from (a). Gray bars denote ideal values, while red (blue) bars indicate positive (negative) experimental correlations. Refer to the Supplemental Material for detailed data with measurement errors. (c) Correlation measurements in plaquettes p_1 to p_8 for Paths 1 and 6. (d) Pauli components corresponding to B_p operators for various braiding paths.

For comparison, the results at vertex v_3 are shown in the lower panel of Fig. 3(a), where all paths lead to the same oscillation curve as there is no e particle excitation at this vertex. The results for $\mathcal{C}_{v_2}$ is similar to that of $\mathcal{C}_{v_1}$ and can be found in [76]. We further analyze the form of the correlation defined in Eq. (3) and extract Pauli operator components from the data in Fig. 3(a). For $\mathcal{C}_v(\gamma)$ at a vertex, we observe that the Pauli components containing σ_z or $\mathbb{I}$ have zero contribution to the expectation value. In addition, each σ_x on a qubit appears as a multiplier $-\sin\gamma$ in the corresponding term, and each σ_y as $\cos\gamma$. Therefore, Pauli components with the same quantity but a different order of σ_x and σ_y add together in terms of the final expectation value as a consequence of measurement symmetry. A new unordered notation are introduced for them, for example using X^4 to denote the value of $\langle\sigma_x^1\sigma_x^2\sigma_x^3\sigma_x^4\rangle$. For measuring $\mathcal{C}_v(\gamma)$, we hence consider the Pauli components X^4 (which is the A_v operator itself), X^3Y, X^2Y^2, XY^3, and Y^4, corresponding to trigonometric terms $\sin^4\gamma$, $\sin^3\gamma\cos\gamma$, $\sin^2\gamma\cos^2\gamma$, $\sin\gamma\cos^3\gamma$, and $\cos^4\gamma$, respectively [76]. Fitting the data to trigonometric functions of γ, we extract the weights of the corresponding Pauli components in the reduced density matrices of the quantum states; see Fig. 3(b). Because the excited state only contains a pair of e particles on vertices v_1 and v_2, only the measurement results on these two vertices reveal the phase change induced by different braiding paths (see the left column for $\mathcal{C}_{v_1}$), and the result for $\mathcal{C}_{v_3}$ is invariant for all braiding paths (right column). These Pauli components provide an efficient way to verify the path-independent nature of the anyonic braiding statistics.

The experimental results for $\mathcal{C}_p(\gamma)$, which reflect the dynamics of stabilizers B_p, are shown in Fig. 3(c). The underlying lattice has eight $\mathcal{C}_p(\gamma)$ operators corresponding to B_1 to B_8 in Fig. 1(a). Their oscillation dynamics can be fitted similar to $\mathcal{C}_v(\gamma)$ [76]. Theoretically, the six different braiding paths should not affect the $\mathcal{C}_p(\gamma)$ operator. Here, we show one nontrivial loop (Path 1) and one trivial loop (Path 6) in Fig. 3(c). The resemblance between the results along these two paths for any of the eight $\mathcal{C}_p(\gamma)$ operators suggests the B_p operators are not disturbed by the braiding scheme. The results for the other braiding paths are shown in [76]. Similar to Fig. 3(b), we can also extract the weights of different Pauli components for $\mathcal{C}_p(\gamma)$, as shown in Fig. 3(d). We can clearly see that the data along all six paths are similar to each other, suggesting that the B_p operators are not disturbed by the braiding scheme, as expected.

In Fig. 3(a), the nontrivial loops (Paths 1, 2, and 5) show the same oscillation dynamics and the system evolves back to the ground state (gray curve) after the anyon

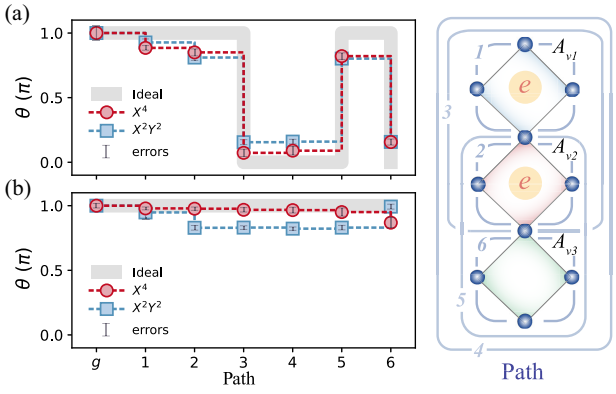

FIG. 4. Extracted phase θ from A_{v1} (a) and A_{v3} (b) along various paths (with included errors). The right diagram illustrates anyon excitations and their braiding paths.

annihilation, with an accumulated phase of π. In contrary, the rest trivial paths (Paths 3, 4, and 6) behave in a different way from the ground state, as the system is left in the excited state after the anyon annihilation. The extracted coefficients of the Pauli components, X^4 and X^2Y^2, as shown in Fig. 3(b), encode the phase value in terms of $\cos\theta$ [76]. The braiding phase can then be experimentally determined. In Fig. 4, the phases θ are listed for all six braiding paths, from which we can clearly verify the path-independent nature of the anyonic braiding statistics.

In conclusion, our experiment utilizes a modular superconducting quantum processor tailored to mimic the physical structure of the toric code model. Through in-parallel control across separate modules, we achieve hardware efficient preparation of the highly entangled ground state and identification of accumulated phases along different paths via correlation measurements, revealing the path-independent nature of anyonic statistics. Further progress in this direction may allow nontrivial connectivity between different modules, creating a compact toric code with closed boundary in real space. Our work sets a precedent for simulating topological phases with modular quantum processors, paving the way for quantum simulation in a distributed fashion.

We thank Keren Li for helpful discussions. This work was supported by the Key-Area Research and Development Program of Guangdong Province (2018B030326001), the National Natural Science Foundation of China (U1801661, 12174178, 12075110, 12374474), the National Key Research and Development Program of China (2019YFA0308100), the Guangdong Innovative and Entrepreneurial Research Team Program (2016ZT06D348, 2019ZT08C044), the Guangdong Provincial Key Laboratory (2019B121203002), the Science, Technology and Innovation Commission of Shenzhen Municipality (KYTD PT20181011104202253, KQTD20210811090049034, KQTD20190929173815000, JCYJ20200109140803865, KQTD20210811090049034), the Shenzhen-Hong Kong Cooperation Zone for Technology and Innovation (HZQB-KCZYB-2020050), the NSF of Beijing (Z190012) and the Guangdong Basic and Applied Basic Research Foundation (2022A1515110615), and the Innovation Program for Quantum Science and Technology (2021ZD0301703).

*These authors contributed equally to this work.
†niujj@sustech.edu.cn
‡zhongyp@sustech.edu.cn
§ludw@sustech.edu.cn

[1] X.-G. Wen, Int. J. Mod. Phys. B **04**, 239 (1990).
[2] K. v. Klitzing, G. Dorda, and M. Pepper, Phys. Rev. Lett. **45**, 494 (1980).
[3] Z.-C. Gu and X.-G. Wen, Phys. Rev. B **80**, 155131 (2009).
[4] A. Kitaev, Ann. Phys. (Amsterdam) **303**, 2 (2003).
[5] M. Dolev, M. Heiblum, V. Umansky, A. Stern, and D. Mahalu, Nature (London) **452**, 829 (2008).
[6] Y. Kasahara, T. Ohnishi, Y. Mizukami, O. Tanaka, S. Ma, K. Sugii, N. Kurita, H. Tanaka, J. Nasu, Y. Motome *et al.*, Nature (London) **559**, 227 (2018).
[7] H. Bartolomei, M. Kumar, R. Bisognin, A. Marguerite, J.-M. Berroir, E. Bocquillon, B. Plaçais, A. Cavanna, Q. Dong, U. Gennser *et al.*, Science **368**, 173 (2020).
[8] S. D. Bartlett, Science **374**, 1200 (2021).
[9] G. Moore and N. Read, Nucl. Phys. **B360**, 362 (1991).
[10] D. A. Ivanov, Phys. Rev. Lett. **86**, 268 (2001).
[11] M. Iqbal, N. Tantivasadakarn, R. Verresen, S. L. Campbell, J. M. Dreiling, C. Figgatt, J. P. Gaebler, J. Johansen, M. Mills, S. A. Moses *et al.*, arXiv:2305.03766.
[12] Y.-J. Hai, Z. Zhang, H. Zheng, L. Kong, J. Wu, and D. Yu, Natl. Sci. Rev. **10**, nwac264 (2022).
[13] B. I. Halperin, Phys. Rev. Lett. **52**, 1583 (1984).
[14] A. Kitaev, Ann. Phys. (Amsterdam) **321**, 2 (2006).
[15] H. Bombin, Phys. Rev. Lett. **105**, 030403 (2010).
[16] A. Stern, Ann. Phys. (Amsterdam) **323**, 204 (2008).
[17] Z. Zhang, X. Long, X. Zhao, Z. Lin, K. Tang, H. Liu, X. Yang, X. Nie, J. Wu, J. Li *et al.*, Phys. Rev. A **105**, L030402 (2022).
[18] X. G. Wen, Phys. Rev. Lett. **66**, 802 (1991).
[19] P. Bonderson, A. Kitaev, and K. Shtengel, Phys. Rev. Lett. **96**, 016803 (2006).
[20] C. Nayak, S. H. Simon, A. Stern, M. Freedman, and S. Das Sarma, Rev. Mod. Phys. **80**, 1083 (2008).
[21] A. Stern, Nature (London) **464**, 187 (2010).
[22] J. Alicea, Y. Oreg, G. Refael, F. von Oppen, and M. P. A. Fisher, Nat. Phys. **7**, 412 (2011).
[23] Q. Wu, A. A. Soluyanov, and T. Bzdušek, Science **365**, 1273 (2019).
[24] Y. Yang, C. Peng, D. Zhu, H. Buljan, J. D. Joannopoulos, B. Zhen, and M. Soljačić, Science **365**, 1021 (2019).
[25] B. Jiang, A. Bouhon, Z.-K. Lin, X. Zhou, B. Hou, F. Li, R.-J. Slager, and J.-H. Jiang, Nat. Phys. **17**, 1239 (2021).
[26] N. Tantivasadakarn, R. Verresen, and A. Vishwanath, Phys. Rev. Lett. **131**, 060405 (2023).
[27] Y. D. Lensky, K. Kechedzhi, I. Aleiner, and E.-A. Kim, Ann. Phys. (Amsterdam) **452**, 169286 (2023).
[28] R. Barends, J. Kelly, A. Megrant, A. Veitia, D. Sank, E. Jeffrey, T. C. White, J. Mutus, A. G. Fowler, B. Campbell *et al.*, Nature (London) **508**, 500 (2014).
[29] Y. Zhou, K. Kanoda, and T.-K. Ng, Rev. Mod. Phys. **89**, 025003 (2017).
[30] M. Sameti, A. Potočnik, D. E. Browne, A. Wallraff, and M. J. Hartmann, Phys. Rev. A **95**, 042330 (2017).
[31] C. Broholm, R. J. Cava, S. A. Kivelson, D. G. Nocera, M. R. Norman, and T. Senthil, Science **367**, eaay0668 (2020).
[32] R. Verresen, M. D. Lukin, and A. Vishwanath, Phys. Rev. X **11**, 031005 (2021).
[33] G. Semeghini, H. Levine, A. Keesling, S. Ebadi, T. T. Wang, D. Bluvstein, R. Verresen, H. Pichler, M. Kalinowski, R. Samajdar *et al.*, Science **374**, 1242 (2021).

[34] Y.-a. Fan, Y. Li, Y. Hu, Y. Li, X. Long, H. Liu, X. Yang, X. Nie, J. Li, T. Xin *et al.*, arXiv:2210.12145.

[35] Y. Zhao, Y. Ye, H.-L. Huang, Y. Zhang, D. Wu, H. Guan, Q. Zhu, Z. Wei, T. He, S. Cao *et al.*, Phys. Rev. Lett. **129**, 030501 (2022).

[36] Z. Wang, Z.-Y. Ge, Z. Xiang, X. Song, R.-Z. Huang, P. Song, X.-Y. Guo, L. Su, K. Xu, D. Zheng, and H. Fan, Phys. Rev. Res. **4**, L022060 (2022).

[37] J. del Pino and O. Zilberberg, Phys. Rev. Lett. **130**, 171901 (2023).

[38] Y. Zhong, D. Xu, P. Wang, C. Song, Q. Guo, W. Liu, K. Xu, B. Xia, C.-Y. Lu, S. Han *et al.*, Phys. Rev. Lett. **117**, 110501 (2016).

[39] C. Song, D. Xu, P. Zhang, J. Wang, Q. Guo, W. Liu, K. Xu, H. Deng, K. Huang, D. Zheng *et al.*, Phys. Rev. Lett. **121**, 030502 (2018).

[40] C.-Y. Lu, X.-Q. Zhou, O. Gühne, W.-B. Gao, J. Zhang, Z.-S. Yuan, A. Goebel, T. Yang, and J.-W. Pan, Nat. Phys. **3**, 91 (2007).

[41] C.-Y. Lu, W.-B. Gao, O. Gühne, X.-Q. Zhou, Z.-B. Chen, and J.-W. Pan, Phys. Rev. Lett. **102**, 030502 (2009).

[42] Z. Luo, J. Li, Z. Li, L.-Y. Hung, Y. Wan, X. Peng, and J. Du, Nat. Phys. **14**, 160 (2017).

[43] C. Liu, H.-L. Huang, C. Chen, B.-Y. Wang, X.-L. Wang, T. Yang, L. Li, N.-L. Liu, J. P. Dowling, T. Byrnes, C.-Y. Lu, and J.-W. Pan, Optica **6**, 264 (2019).

[44] J. Noh, T. Schuster, T. Iadecola, S. Huang, M. Wang, K. P. Chen, C. Chamon, and M. C. Rechtsman, Nat. Phys. **16**, 989 (2020).

[45] X.-L. Zhang, F. Yu, Z.-G. Chen, Z.-N. Tian, Q.-D. Chen, H.-B. Sun, and G. Ma, Nat. Photonics **16**, 390 (2022).

[46] G. Feng, G. Long, and R. Laflamme, Phys. Rev. A **88**, 022305 (2013).

[47] A. J. Park, E. McKay, D. Lu, and R. Laflamme, New J. Phys. **18**, 043043 (2016).

[48] K. Li, Y. Wan, L.-Y. Hung, T. Lan, G. Long, D. Lu, B. Zeng, and R. Laflamme, Phys. Rev. Lett. **118**, 080502 (2017).

[49] H.-N. Dai, B. Yang, A. Reingruber, H. Sun, X.-F. Xu, Y.-A. Chen, Z.-S. Yuan, and J.-W. Pan, Nat. Phys. **13**, 1195 (2017).

[50] J. Nakamura, S. Liang, G. C. Gardner, and M. J. Manfra, Nat. Phys. **16**, 931 (2020).

[51] K. J. Satzinger, Y.-J. Liu, A. Smith, C. Knapp, M. Newman, C. Jones, Z. Chen, C. Quintana, X. Mi, A. Dunsworth *et al.*, Science **374**, 1237 (2021).

[52] N. Harle, O. Shtanko, and R. Movassagh, Nat. Commun. **14**, 2286 (2023).

[53] T. I. Andersen, Y. D. Lensky, K. Kechedzhi, I. K. Drozdov, A. Bengtsson, S. Hong, A. Morvan, X. Mi, A. Opremcak, R. Acharya *et al.*, Nature (London) **618**, 264 (2023).

[54] S. Xu, Z.-Z. Sun, K. Wang, L. Xiang, Z. Bao, Z. Zhu, F. Shen, Z. Song, P. Zhang, W. Ren *et al.*, Chin. Phys. Lett. **40**, 060301 (2023).

[55] R. Acharya, I. Aleiner, R. Allen, T. I. Andersen, M. Ansmann, F. Arute, K. Arya, A. Asfaw, J. Atalaya, R. Babbush *et al.*, Nature (London) **614**, 676 (2023).

[56] R.-R. Du, Nat. Phys. **16**, 899 (2020).

[57] S. Scheel and A. Szameit, Nat. Photonics **16**, 344 (2022).

[58] J.-Y. M. Lee, C. Hong, T. Alkalay, N. Schiller, V. Umansky, M. Heiblum, Y. Oreg, and H.-S. Sim, Nature (London) **617**, 277 (2023).

[59] M. Parto, C. Leefmans, J. Williams, F. Nori, and A. Marandi, Nat. Commun. **14**, 1440 (2023).

[60] H. K. Kundu, S. Biswas, N. Ofek, V. Umansky, and M. Heiblum, Nat. Phys. **19**, 515 (2023).

[61] Y.-J. Han, R. Raussendorf, and L.-M. Duan, Phys. Rev. Lett. **98**, 150404 (2007).

[62] F. Arute, K. Arya, R. Babbush, D. Bacon, J. C. Bardin, R. Barends, R. Biswas, S. Boixo, F. G. S. L. Brandao, D. A. Buell *et al.*, Nature (London) **574**, 505 (2019).

[63] M. Gong, S. Wang, C. Zha, M.-C. Chen, H.-L. Huang, Y. Wu, Q. Zhu, Y. Zhao, S. Li, S. Guo *et al.*, Science **372**, 948 (2021).

[64] P. Zhang, H. Dong, Y. Gao, L. Zhao, J. Hao, J.-Y. Desaules, Q. Guo, J. Chen, J. Deng, B. Liu *et al.*, Nat. Phys. **19**, 120 (2022).

[65] I. Carusotto, A. A. Houck, A. J. Kollár, P. Roushan, D. I. Schuster, and J. Simon, Nat. Phys. **16**, 268 (2020).

[66] B. Cheng, X.-H. Deng, X. Gu, Y. He, G. Hu, P. Huang, J. Li, B.-C. Lin, D. Lu, Y. Lu *et al.*, Front. Phys. **18**, 21308 (2023).

[67] P. Kurpiers, P. Magnard, T. Walter, B. Royer, M. Pechal, J. Heinsoo, Y. Salathé, A. Akin, S. Storz, J.-C. Besse *et al.*, Nature (London) **558**, 264 (2018).

[68] C. J. Axline, L. D. Burkhart, W. Pfaff, M. Zhang, K. Chou, P. Campagne-Ibarcq, P. Reinhold, L. Frunzio, S. M. Girvin, L. Jiang *et al.*, Nat. Phys. **14**, 705 (2018).

[69] P. Campagne-Ibarcq, E. Zalys-Geller, A. Narla, S. Shankar, P. Reinhold, L. Burkhart, C. Axline, W. Pfaff, L. Frunzio, R. J. Schoelkopf *et al.*, Phys. Rev. Lett. **120**, 200501 (2018).

[70] P. Magnard, S. Storz, P. Kurpiers, J. Schär, F. Marxer, J. Lütolf, T. Walter, J.-C. Besse, M. Gabureac, K. Reuer *et al.*, Phys. Rev. Lett. **125**, 260502 (2020).

[71] Y. Zhong, H.-S. Chang, A. Bienfait, É. Dumur, M.-H. Chou, C. R. Conner, J. Grebel, R. G. Povey, H. Yan, D. I. Schuster *et al.*, Nature (London) **590**, 571 (2021).

[72] L. D. Burkhart, J. D. Teoh, Y. Zhang, C. J. Axline, L. Frunzio, M. Devoret, L. Jiang, S. Girvin, and R. Schoelkopf, PRX Quantum **2**, 030321 (2021).

[73] T. Monz, P. Schindler, J. T. Barreiro, M. Chwalla, D. Nigg, W. A. Coish, M. Harlander, W. Hänsel, M. Hennrich, and R. Blatt, Phys. Rev. Lett. **106**, 130506 (2011).

[74] A. Omran, H. Levine, A. Keesling, G. Semeghini, T. T. Wang, S. Ebadi, H. Bernien, A. S. Zibrov, H. Pichler, S. Choi, J. Cui, M. Rossignolo, P. Rembold *et al.*, Science **365**, 570 (2019).

[75] M. Levin and X.-G. Wen, Phys. Rev. Lett. **96**, 110405 (2006).

[76] See Supplemental Material at http://link.aps.org/supplemental/10.1103/PhysRevLett.132.020601 for the system parameters and experimental details.

[77] J. Niu, L. Zhang, Y. Liu, J. Qiu, W. Huang, J. Huang, H. Jia, J. Liu, Z. Tao, W. Wei *et al.*, Nat. Electron. **6**, 235 (2023).